Chemical profile and magnetoresistance of $Ga_{1-x}Mn_xAs/GaAs/AlAs/GaAs/Ga_{1-x}Mn_xAs$ tunnel junctions

R. Mattana,* M. Elsen, J.-M. George,† H. Jaffrès, F. Nguyen Van Dau, and A. Fert
Unité Mixte de Physique CNRS-THALES, Domaine de Corbeville, 91404 Orsay Cedex, France and Université Paris Sud, 91405 Orsay Cedex, France

M. F. Wyczisk, J. Olivier, and P. Galtier
THALES Research and Technology France, Domaine de Corbeville, 91404 Orsay Cedex, France

B. Lépine, A. Guivarc'h, and G. Jézéquel
Equipe de Physique des Surfaces et Interfaces, Unité Mixte de Recherche CNRS-Université 6627 "PALMS," Université Rennes I, 35042 Rennes Cedex, France

(Received 25 June 2004; revised manuscript received 19 November 2004; published 25 February 2005)

We have investigated the manganese diffusion depth and the tunneling magnetoresistance (TMR) properties in $Ga_{1-x}Mn_xAs/GaAs/AlAs/GaAs/Ga_{1-x}Mn_xAs$ tunnel junctions. Auger electron spectroscopy and transmission electron microscopy analysis show that the Mn diffusion depth is less than 15 Å. TMR measurements have been performed on tunnel junctions where different GaAs spacer thicknesses are inserted between the $Ga_{1-x}Mn_xAs$ electrode and AlAs tunnel barrier. Our results suggest that the GaAs thickness plays a crucial role on the temperature dependence of the TMR.

DOI: 10.1103/PhysRevB.71.075206 PACS number(s): 66.30.Jt, 72.25.Dc, 73.43.Jn

I. INTRODUCTION

Electrical spin manipulation in semiconductors constitutes a huge challenge for a new generation of spin-electronic devices.[1] Tunnel junctions based on ferromagnetic semiconductors are of great interest because the existence of tunnel magnetoresistance (TMR) is a signature of the transmission of spin-polarized carriers.[2] Magnetic tunnel junctions (MTJ's) based on the $Ga_{1-x}Mn_xAs$ ferromagnetic semiconductor[3,4] have been studied by several groups[5,6] in recent years. Although this ferromagnetic semiconductor[7] has a relatively weak Curie temperature, currently reaching 159 K,[8] it is relatively easily integrated into III-V semiconductor heterostructures. Therefore $Ga_{1-x}Mn_xAs$-based MTJ's constitute a reference system for future electrical spin manipulation experiments. In tunnel junctions, the insertion of a thin GaAs spacer ($\sim$10 Å) between the $Ga_{1-x}Mn_xAs$ ferromagnetic electrodes and the AlAs tunnel barrier has been found to significantly enhance the TMR.[9] It seems that this GaAs spacer prevents Mn diffusion into the tunnel barrier and therefore improves TMR. Since the results published by Tanaka and Higo,[9] several groups have introduced this GaAs layer in similar structures [$Ga_{1-x}Mn_xAs/AlAs/GaAs/AlAs/Ga_{1-x}Mn_xAs$ (Ref. 10) and $Ga_{1-x}Mn_xAs/AlAs/MnAs$ (Ref. 11)]. These results raise different questions about the Mn diffusion depth and the influence on the TMR of a GaAs layer inserted between ferromagnetic (FM) electrodes and an insulator (I) tunnel barrier.

In this paper, we investigate the chemical profile of $Ga_{1-x}Mn_xAs/GaAs/AlAs/GaAs/Ga_{1-x}Mn_xAs$ tunnel junctions. The manganese diffusion depth at the $Ga_{1-x}Mn_xAs/GaAs$ interface is determined by Auger electron spectroscopy (AES) and transmission electron microscopy analysis. Then we discuss the spin-dependent transport properties of magnetic tunnel junctions. In particular, we study the temperature dependence of TMR in tunnel junctions when GaAs spacer layers, thicker than the Mn diffusion depth, are inserted at the ferromagnetic-insulator interfaces. The tunnel junctions studied are composed of two $Ga_{1-x}Mn_xAs$ ferromagnetic electrodes separated by a thin AlAs (17 Å) tunnel barrier. In order to determinate the Mn diffusion depth we have inserted a 100-Å-thick GaAs layer at the FM/I interfaces. Magnetic and electrical measurements have been performed on magnetic tunnel junctions with thinner GaAs spacer layers of 10 Å and 50 Å. MTJ's have not been annealed in order to prevent Mn diffusion into the whole heterostructures.

II. SAMPLE PREPARATION

A. Growth procedure

Samples were prepared in a RIBER 2300 molecular beam epitaxy (MBE) system equipped with an As_4 solid source. We used semi-insulating GaAs(001) wafers on which a 100-nm-thick undoped GaAs buffer was first grown at high temperature using standard conditions [substrate at 580 °C, ratio between the beam equivalent pressures (BEP) of As_4 and Ga equal to $\sim$ 25, growth rate of 0.3 μm/h]. The growth of $Ga_{1-x}Mn_xAs$ was then initiated at 230 °C on a C 4×4 As-rich GaAs surface with the same rate but an As_4/Ga BEP ratio equal to 10. During and after the growth, reflection high-energy electron diffraction (RHEED) showed a streaked pattern with a 1×2 surface reconstruction. The magnetic tunnel junctions with 10-, 50- and 100-Å GaAs spacer thicknesses were grown under the same conditions.

TABLE I. Crystallographic data of $Ga_{1-x}Mn_xAs$ samples: the lattice parameters in the perpendicular ($a_\perp$) and parallel ($a_\parallel$) directions to the sample surface were determined from the measurement of the (004) and (444) plane reticular distances. The relaxed (bulk) lattice parameter (a_0) was calculated with the C_{11} and C_{12} elastic moduli of GaAs (Ref. 14).

x_{Mn} (%)	d(004) (nm)	d(444) (nm)	$a_\perp$ (nm)	$a_\parallel$ (nm)	a_0 bulk (nm)
0	0.14141	0.08161	0.5656	0.5653	0.5655
3.7	0.14185	0.08170	0.5674	0.5654	0.5664
6.6	0.14219	0.08176	0.5688	0.5653	0.5671
7.1	0.14225	0.08178	0.5690	0.5653	0.5673

B. $Ga_{1-x}Mn_xAs$ electrode characterizations

1. X-ray diffraction measurements

Calibration samples of 1 μm thick were made at different Mn compositions: $x=0,0.037,0.066,0.071$. Note that the $x=0$ sample was used as a reference for the low-temperature GaAs growth. The Mn composition was determined by energy dispersive analysis of X-rays (EDX) and the structural properties of the layers were studied by X-ray diffraction on a $\omega-2\theta$ diffractometer (CGR Theta 2000) equipped with a front curved quartz monochromator ($\lambda_{CuK\alpha 1}=0.154\,056$ nm).

Results of the X-ray diffraction measurements are summarized in Table I. The (004) reflection was analyzed in the usual symmetrical geometry θ–2θ and the (444) reflection in an asymmetrical geometry ω–2θ [$\omega=\theta-\psi$ with θ the Bragg angle and ψ the angle between the sample surface and the (444) planes]. The corresponding reticular distances allowed the calculation of the lattice parameters of the $Ga_{1-x}Mn_xAs$/GaAs layers in the perpendicular ($a_\perp$) and parallel ($a_\parallel$) directions to the sample surface. For all Mn compositions, $a_\parallel$ is equal to the lattice parameter of the substrate (0.565 33 nm) taking into account the accuracy of our measurements (1.5×10^{-4} on $a_\parallel$). These 1-μm-thick layers are thus fully strained to the GaAs(001) substrate and undergo a compressive stress.[12,13] From these results, we have calculated their relaxed (bulk) lattice parameter (a_0) assuming that $Ga_{1-x}Mn_xAs$ has the same elastic constants as GaAs in this Ga-rich composition range.[14]

Figure 1 shows a linear dependence of a_0 with Mn composition that is in good agreement with the previous works of Shott *et al.*[15] (MBE growth at 220 °C) and Sadowski *et al.*[16] (MBE at 200 °C or migration-enhanced epitaxy at 150 °C for $8\%\leqslant x\leqslant 10\%$). However, this behavior is quite different to the one observed by Ohno *et al.*[17] (MBE at 250 °C) but was shown to depend strongly on the excess As incorporation during growth.[12,15]

2. Magnetic and electrical measurements

$Ga_{1-x}Mn_xAs$ layers exhibit magnetic and transport properties similar to those already reported by Ohno,[18] leading to a qualitative agreement with the proposed phase diagram. Figure 2(a) shows the variation of the magnetic moment as a function of temperature (T) corresponding to three different concentrations and Fig. 2(b) displays the variation of the resistivity of two characteristic samples. This last figure clearly illustrates the metal-insulator transition occurring when the Mn concentration reaches 4.8%. At low concentration ($x\leqslant 4\%$), an exponential variation of the magnetization versus T can be observed, thus illustrating a weak ferromagnetic phase. This low concentration limit is also characterized by an insulating phase [Fig. 2(b)] by which a variation of 5 orders of magnitude on the resistivity is observed when cooling down the sample from room temperature to 10 K. This phase displays a low Curie temperature (about 35 K) whose behavior may be attributed to polaron percolation.[19] At higher concentration, the metallic phase is achieved correspondingly to a Curie temperature larger than 60 K. With our growth conditions, the solubility limit is reached at a concentration of $x\geqslant 6.25\%$, above which the formation of MnAs cluster occurs. This effect is seen in Fig. 2(a) where, for the highest Mn concentration, a magnetic phase persists until room temperature, indicating the presence of a MnAs compound ($T_C=340$ K).

III. CHEMICAL PROFILE

A. Transmission electron microscopy

Transmission electron microscopy (TEM) was performed on tunnel junction with 100-Å-thick GaAs layers. See Table II for sample characteristics. Due to the low Mn concentration and the small mass difference between Mn and Ga, a

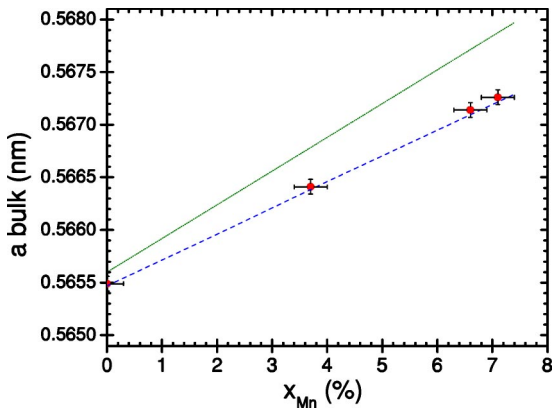

FIG. 1. (Color online) Relaxed (bulk) lattice parameter of $Ga_{1-x}Mn_xAs$ vs composition. Our experimental points are compared to the data obtained by Ohno *et al.* (Ref. 17) (in short dots) and Sadowski *et al.* (Ref. 16) or Shott *et al.* (Ref. 15) (same curve in dashed line).

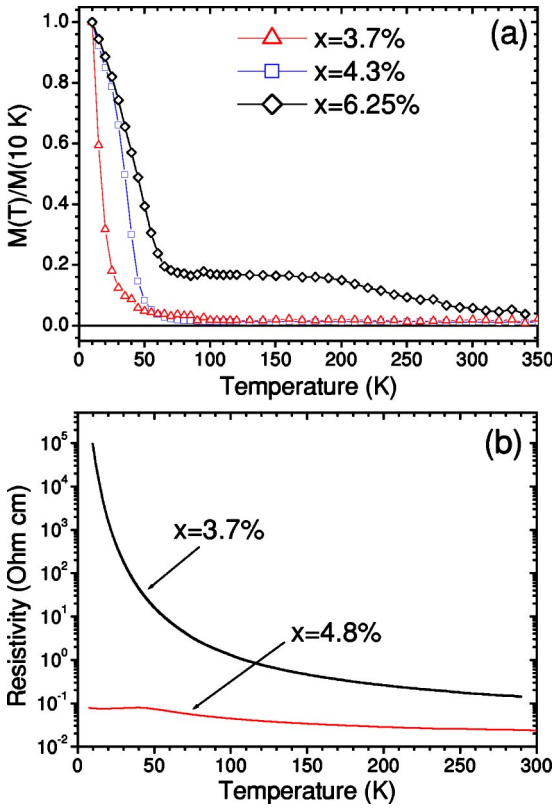

FIG. 2. (Color online) (a) Normalized magnetization of a 1 -μm $Ga_{1-x}Mn_xAs$ layer with $x=3.7\%$, 4.3%, 6.25% as a function of the temperature. (b) Resistivity as a function of the temperature in the "current in plane" geometry for layers of $Ga_{1-x}Mn_xAs$ with $x=3.7\%$ and 4.8%.

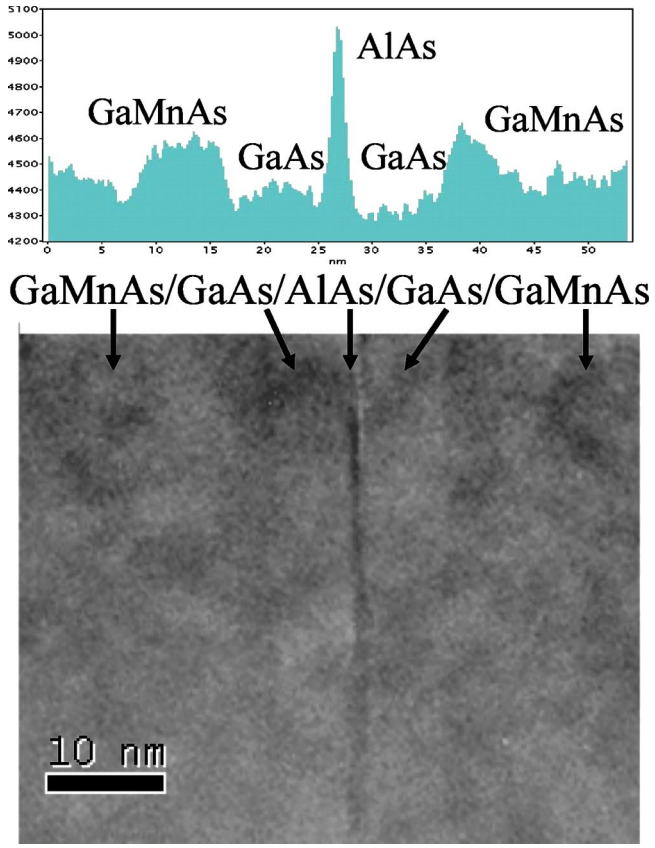

FIG. 3. (Color online) TEM image of the tunnel junction with 100-Å-thick GaAs and the extracted intensity variation related to the different layers.

relatively weak contrast is expected, and thus the observation was performed on a cleaved corner. In this geometry (i) the observation direction is [001], which is very sensitive to the chemical composition and (ii) the geometry allows the visualization of a small concentration related to the contrast variation along the sample thickness. A bright field image obtained with a resolution of 5 Å is shown (Fig. 3) where the $Ga_{1-x}Mn_xAs/GaAs/AlAs/GaAs/Ga_{1-x}Mn_xAs$ structure is clearly visible. Despite the weak contrast at the $GaAs/Ga_{1-x}Mn_xAs$ interface, an interface sharpness of about 10 Å is deduced from the intensity variation (upper panel of Fig. 3).

B. Auger electron spectroscopy

Auger electron spectroscopy (AES) constitutes a good surface spectroscopy because the escape depth of the Auger electrons is in the range of 0.5–3 nm. Combined with ion etching, AES can be used to obtain elemental concentration profiles within overlayers. Nevertheless, several factors affect the resolution depth. The most important mechanisms that broaden the concentration profiles can be divided into two classes: Auger electron escape depth and ion bombardment effects (ion knock-on mixing and ion-induced roughness).

(i) In an Auger sputter profiling experiment, the measured elemental signal strength represents an average concentration in the surface region of thickness L. Thus, the depth resolution is limited by the escape depth and will be optimum if the escape depth is minimized.

(ii) First, ions incident on a specimen surface create an atomic collision cascade in the bulk of the material. Some atoms in this cascade reach the surface and are sputtered. Primary recoils are displaced into deeper layers (knock-on

TABLE II. Characteristics of samples studied. Thickness of bottom ($Ga_{1-x}Mn_xAs$) and top ($Ga_{1-y}Mn_yAs$) electrodes are, respectively, 300 nm and 30 nm and the AlAs barrier thickness is 1.7 nm.T_{C_x} (K) and T_{C_y} (K) denote the Curie temperatures of the bottom and top ($Ga_{1-x}Mn_xAs$) electrodes.

Samples	Structure	x (%)	y (%)	T_{C_x} (K)	T_{C_y} (K)
AlAs barrier	$Ga_{1-x}Mn_xAs$/GaAs(10 Å)/AlAs/GaAs(10 Å)/$Ga_{1-y}Mn_yAs$	4.5	5.7	45	45
GaAs/AlAs/GaAs barrier	$Ga_{1-x}Mn_xAs$/GaAs(50 Å)/AlAs/GaAs(50 Å)/$Ga_{1-y}Mn_yAs$	5.4	6.1	55	90
TEM and AES	$Ga_{1-x}Mn_xAs$/GaAs(100 Å)/AlAs/GaAs(100 Å)/$Ga_{1-y}Mn_yAs$	4.3	5.3	35	35

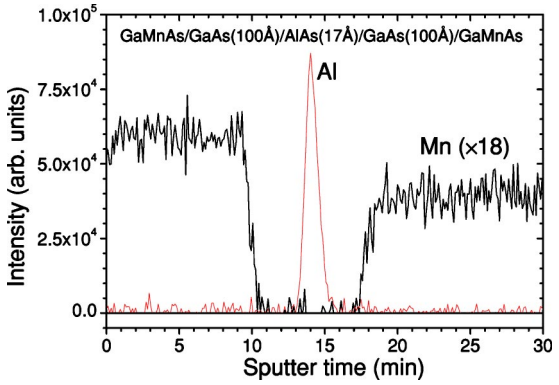

FIG. 4. (Color online) Rough spectra obtained at 500 eV. Auger signals of the manganese and aluminum are plotted.

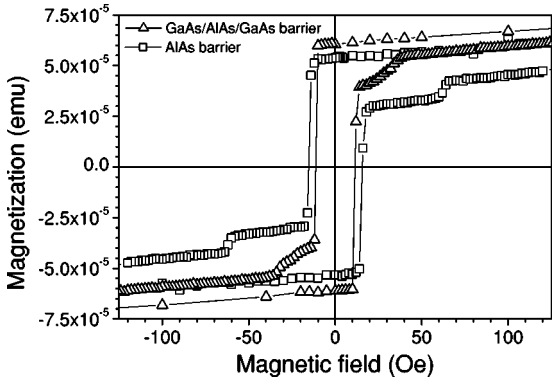

FIG. 5. Magnetic measurements performed at 10 K on tunnel junctions with AlAs barrier (squares) and GaAs/AlAs/GaAs barrier (triangles). The magnetic field is applied in the plane, along the [100] axis.

effect) and the other atoms are displaced from their original position (atomic mixing), resulting in a broadening of the measured depth profile. Second, it is known that a number of projectile-target combinations leads to a roughening of the surface during sputtering, depending on the ion-target nature, on impurities present on the surface, on the ion energy, dose, and incidence angle. It is apparent that the depth resolution of composition profiling methods will be degraded by the development of topographical structures.

The measured interface width (W_m) is defined in the Auger depth profile as the distance between two points wherein the auger signal varies from 84% to 16% of its total change across the interface. The true interface width (W_t) can be extracted from Auger profile depth taking into account the broadening terms due to mixing (X_M) and roughening (X_R), the escape depth L, and the geometry of the electron energy analysis, α. The measured interface width can be written[20]

$$W_m = (W_t^2 + \alpha^2 L^2 + X_M^2 + X_R^2)^{1/2}. \quad (1)$$

A 500-eV (280 nA) and a 1-keV (350 nA) Ar^+ ion beam were used to etch the sample during Auger concentration profiling (5 keV, 20 nA). We have used also a scanning force microscope which investigates the surface structures at the atomic level in order to precisely measure the surface roughness. In good agreement with results obtained on the interfaces GaAs/$Al_xGa_{1-x}As$ and $Al_xGa_{1-x}As$/GaAs,[21,22] in the 150-nm range of etched material depth, the $Ga_{1-x}Mn_xAs$ surface roughness remains nearly constant and equal to ~0.6nm. From raw spectrum obtained at 1 keV and 500 eV (Fig. 4), the manganese diffusion depth at the $Ga_{1-x}Mn_xAs$ /GaAs and GaAs/$Ga_{1-x}Mn_xAs$ interfaces can be evaluated to 12±3 Å.

Taking into account the Mn diffusion depth, established by AES analysis, we have elaborated a magnetic tunnel junction with a GaAs spacer thicker (50 Å) than the Mn diffusion depth (~12±3 Å) in order to study the influence of a nonmagnetic semiconductor layer inserted at the FM/I interfaces on the TMR. Magnetotransport experiments performed on this junction (namely GaAs/AlAs/GaAs barrier) are compared to results obtained on MTJ with only 10-Å-thick GaAs spacer (namely AlAs barrier).

IV. SPIN-DEPENDENT TRANSPORT

A. Experimental results

We now focus on the spin-polarized transport in such tunnel junctions. The top and bottom $Ga_{1-x}Mn_xAs$ ferromagnetic electrodes have different thickness (30 and 300 nm) and different Mn concentration (6.1% and 5.4% for the MTJ with a 50-Å GaAs spacer and 5.3% and 4.3% for the MTJ with a 10-Å GaAs spacer) in order to obtain two different coercive fields and thus an antiparallel (AP) magnetic configuration. Magnetic measurements show that the Curie temperature is, respectively, 90 and 55 K (for the top and bottom electrodes) for the GaAs/AlAs/GaAs barrier sample and 45 K for AlAs barrier sample.

Figure 5 represents the hysteresis loops recorded by superconducting quantum interference device (SQUID) measurement at 10 K on the $Ga_{1-x}Mn_xAs$/GaAs/AlAs/GaAs/$Ga_{1-x}Mn_xAs$ sample before patterning. The magnetic field is applied in the plane of the layer along the [100] direction. For all the structures, an easy axis was observed in this peculiar direction, leading to an antiparallel arrangement of the magnetic $Ga_{1-x}Mn_xAs$ layers in the range of field between 30 and 100 Oe. The value of the magnetic moment in the AP configuration matches the expected value deduced from the ratio of the two $Ga_{1-x}Mn_xAs$ layer thickness.

For the electrical measurements, samples are patterned into circular junctions using optical lithography. The junction diameter varies from 10 to 300 μm. The resistance area (RA) product of tunnel junctions at 1 mV and 4 K is about 0.1 Ω cm^2 for the AlAs barrier (in agreement with the works of Tanaka and Higo[9]) and 25 Ω cm^2 for the GaAs/AlAs/GaAs tunnel barrier. As shown in Figs. 6(a) and 7(a) both structures exhibit a significant magnetoresistance (MR) at low bias with a resistance maximum value corresponding to the AP configuration.

Because the tunnel resistances of junctions is two orders of magnitude larger than the resistance of the $Ga_{1-x}Mn_xAs$ electrode, the MR observed cannot be attributed to anisotropic magnetoresistance effects (AMR) of the ferromagnetic electrodes. In order to better interpret the physical effects, the variation of tunnel resistance versus the in-plane magne-

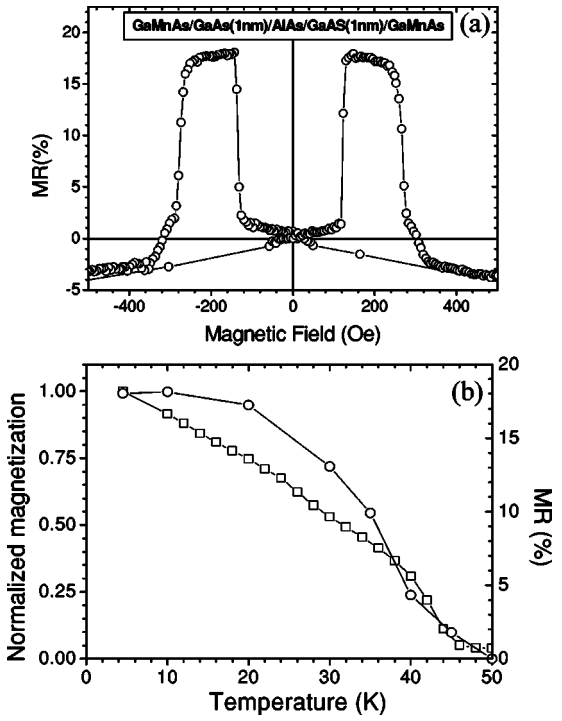

FIG. 6. (a) Magnetoresistance of the tunnel junction containing a 10-Å-thick GaAs spacer measured at 4 K and at a constant bias of 5 mV. (b) Temperature dependence of magnetization (squares, left scale) and magnetoresistance (circle, right scale).

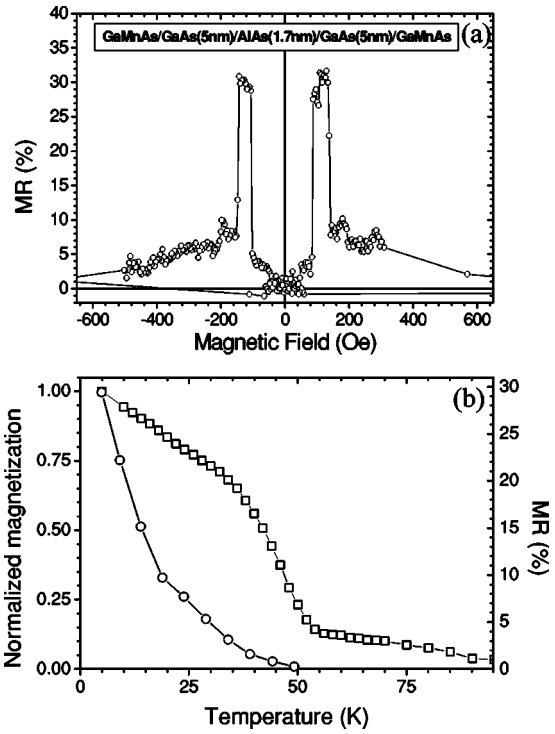

FIG. 7. (a) Magnetoresistance of the junction including 50-Å-thick GaAs measured at 4 K and at a constant bias of 1 mV. (b) Temperature dependence of magnetization (squares, left scale) and magnetoresistance (circle, right scale) of the junction with 50-Å-thick GaAs.

tization direction was recorded in the saturated magnetic state (0.6 T). No variation was observed in the junction with the AlAs barrier and a maximum value of 2% between the [100] easy axis and the [110] hard axis was observed on the GaAs/AlAs/GaAs tunnel junction. This feature rules out tunneling anisotropic magnetoresistance effect as recently reported.[23] From the nonlinear $I(V)$ curves recorded at low temperature (4 K) on both tunnel junctions with 10- and 50-Å-thick GaAs spacer (inset of Fig. 8), we can conclude that a spin-dependent tunnel transport takes place across these structures.

1. Single AlAs tunnel barrier

Figure 6(a) shows the variation of resistance with the magnetic field in plane, along the [100] axis at 4 K and 5 mV. Note that because of the antiferromagnetic dipolar coupling occurring between the two ferromagnetic electrodes after patterning, the AP plateau appears to be enlarged compared to the one measured before patterning (Fig. 5).

For this barrier and in the case of a direct tunneling, the temperature dependence of the magnetoresistance reported in Fig. 6(b) should be linked, through a generalized Jullière formula,[24] to the temperature dependence of the hole spin polarization within the $Ga_{1-x}Mn_xAs$ electrodes. Note that, in this case, TMR follows quite closely the decrease of magnetization to cancel at T_C.

2. GaAs/AlAs/GaAs tunnel barrier

Figure 7(a) shows the variation of resistance with the magnetic field in plane, along the [100] axis, at 4 K and 1 mV. Unlike the single AlAs barrier, the drop of the TMR versus temperature for GaAs/AlAs/GaAs composite barriers is much faster than the decrease of the magnetization [Fig. 7(b)] and thus does not seem to be correlated to the magnon excitations or to the hole spin polarization. The fast vanishing of TMR suggests here that, parallel to a direct spin-dependent tunneling, a non-spin-polarized thermal-assisted transport mechanism is taking part in the tunnel conduction as emphasized in the following section.

Figure 8 displays the normalized TMR bias dependence for the two magnetic tunnel junctions, that is, TMR

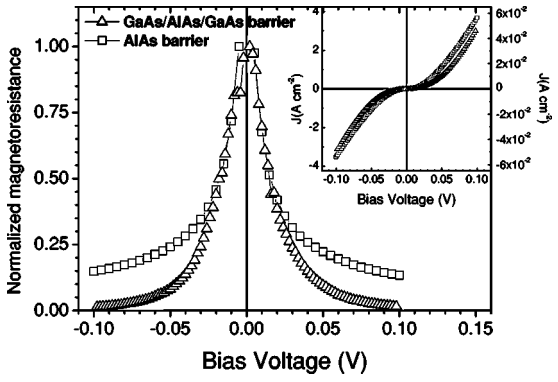

FIG. 8. Bias voltage dependence of magnetoresistance at low temperature of magnetic tunnel junctions with 10- and 50-Å-thick GaAs spacers. In the inset, nonlinear $J(V)$ curves of tunnel junctions with 10-Å- (left scale) and 50-Å-thick (right scale) GaAs at 4 K and at zero field.

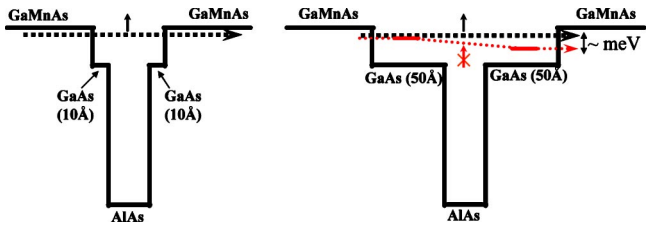

FIG. 9. (Color online) Valence-band profile of magnetic tunnel junctions with 10- and 50-Å-thick GaAs spacers. The dashed line represents direct tunneling through the GaAs/AlAs/GaAs barrier with spin conservation whereas the dotted line represents a two-defect-assisted tunneling associated with spin flip.

(V)/TMR(1 mV). The corresponding decrease of TMR is monotonic with a characteristic $V_{1/2}$ of about 15 mV. The behavior of the bias is quite similar for both types of junctions despite a slightly faster decrease observed for the GaAs/AlAs/GaAs composite barrier above 20 mV.

B. Transport mechanisms

It has been shown by transport measurements[25] and by photoemission[26] that the valence-band offset at the $Ga_{1-x}Mn_xAs$/GaAs interface is still of the order of 100 meV, GaAs also playing the role of a barrier for holes injected from $Ga_{1-x}Mn_xAs$.[27] The resulting shape of the valence band profile (Fig. 9) then makes possible two different tunnel transport mechanisms: direct tunneling from $Ga_{1-x}Mn_xAs$ to $Ga_{1-x}Mn_xAs$ across the GaAs/AlAs/GaAs composite barrier taken as a whole or a defect-assisted tunneling,[28,29] more probable for thick barriers,[30] and for low-temperature grown GaAs,[31–33] where the number of defects is known to increase (As antisites, Ga vacancies, etc.). The relative contribution of such mechanisms is related to the surface defects density[28] and/or to the width of the impurity band beyond the metal-insulator transition (large defect density).

In the case of holes, because the large spin-orbit coupling is associated with a significant spin mixing, we can discriminate three elementary processes[30] according to the number of defects, N, involved for the transport:

(i) A spin-conservative direct tunneling ($N=0$) giving rise to standard TMR effects (hereafter designed as $TMR^{(0)}$) whose amplitude can be linked to the electrode polarization through a Jullière-like model[24] extended to spin-orbit coupled states. The evolution of $TMR^{(0)}$ with temperature (T), barrier thickness, and/or nature must then be associated with a loss or an increase of the effective carrier spin polarization. We think that the spin-dependent tunneling seen on the single AlAs barrier (Fig. 6, Tanaka and Higo[9] and Mattana *et al.*[10]) can be related to such direct tunneling.[34] The decrease of TMR with T reported on Fig. 6(b) must then be ascribed to hole depolarization due to magnon excitations in $Ga_{1-x}Mn_xAs$ when approaching the Curie temperature (T_C).[35] Along the same ideas, the drop of TMR with AlAs barrier thickness[9] must evidence a vanishing spin polarization of holes for thicker barriers.

(ii) A spin-dependent tunneling through a variety of chains including a single (nonmagnetic) localized state[36] ($N=1$), whose probability to be located near the center of the barrier is large. A good example of such a magnetoresistance effect is given by Petukhov *et al.*[37] for the condition of resonant tunneling through a quantized state within a quantum well. However, concerning defect-assisted tunneling, the observation of such resonance[38] is conditioned by a large resonant width (Γ) in comparison to the bias (eV) applied and to the width (W) of the impurity band. These criteria are hardly fulfilled for holes because of a smaller tunnel transmission. The resulting integrated resonant tunneling of spin-polarized carriers gives rise to a TMR (designed as $TMR^{(1)}$) that is half of $TMR^{(0)}$ as calculated in the case of a double junction with a nonmagnetic central electrode.[39] An example of such spin-dependent tunneling process is the TMR signal obtained on $Ga_{1-x}Mn_xAs$/AlAs/GaAs/AlAs/$Ga_{1-x}Mn_xAs$ double junctions[10,35,37] at low temperature (4 K) where the carrier depolarization by hopping-assisted spin flip is quenched.[36,40] Except for a factor of 2 between $TMR^{(0)}$ and $TMR^{(1)}$, the two above-mentioned processes can be hardly discriminated experimentally, having no specific signature in temperature T and bias eV.

(iii) An inelastic tunneling through a variety of chains including several localized states ($N \geqslant 2$) in the barrier. We expect that these mechanisms, predominant for thick barriers, at higher temperature or at higher bias, as shown by Xu *et al.*,[30] are mostly non-spin-conservative because of the strong depolarization occurring through hopping-assisted spin flips between two spin-orbit coupled states. As largely emphasized by Xu *et al.*[30] and references therein in the case of homogeneous barriers, the conductivity associated with such a chain of N localized states has a specific signature in temperature and bias according to $T^{N-1+(N-1)/(N+1)}$ and $eV^{N-1+(N-1)/(N+1)}$. However, a small deviation from these power laws can occur for composite barriers.

The overall tunnel conductivity, σ, is then the sum of the related chain conductivity, $\sigma^{(N)}$ according to $\sigma=\Sigma\sigma^{(N)}$, whereas the resulting TMR is written simply $\sigma \times \mathrm{TMR} = \Sigma\sigma^{(N)} \times \mathrm{TMR}^{(N)}$ or is expressed versus the characteristic resistances:

$$\frac{\mathrm{TMR}}{R} = \sum_N \frac{\mathrm{TMR}^{(N)}}{R^{(N)}} \tag{2}$$

A striking point is the dependence of both TMR and resistance upon T for the GaAs(5 nm)/AlAs/GaAs(5 nm) barrier reported on Fig. 10 by comparison to the reference AlAs barrier. Whereas TMR and resistance in the antiparallel magnetic configuration (R_{AP}) are not correlated for the AlAs barrier, TMR and R_{AP} of the GaAs/AlAs/GaAs composite barrier follow the same variation. This feature could be linked to a linear increase of the conductivity with T (Fig. 10, $R \propto T^{-1}$ or $\sigma \propto T$).

From Eq. (2), such correlation between TMR and resistance, $\mathrm{TMR} \propto R_{AP}$ (Fig. 10), is then compatible with the existence of a spin-dependent tunnel signal mostly nonthermally activated and including no more than a single defect ($N=0$ or $N=1$) shunted by an unpolarized and thermally assisted conduction including at least two defects ($\mathrm{TMR}^{(N)}=0$ and $R \sim T^{-1}$ for $N \geqslant 2$). Consequently, the rapid decrease of

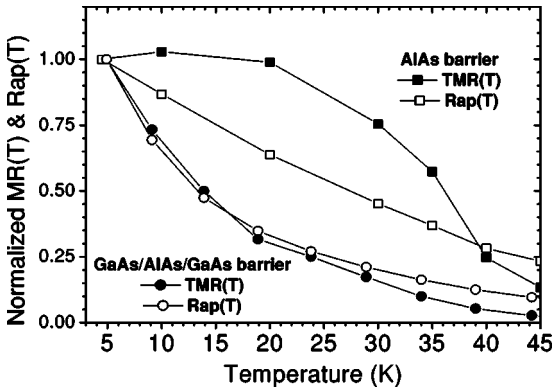

FIG. 10. Temperature dependence of magnetoresistance and resistance in the antiparallel magnetic configuration of junction including respectively 10- and 50-Å-thick GaAs.

TMR for GaAs/AlAs/GaAs junctions below 25 K, which is far from T_C, conjugated to a drop of resistance with T may be attributed to the opening of a nonpolarized thermal channel played by a possible two defect-assisted tunneling required for such valence-band profile (Fig. 9). This scenario is also supported by the faster decrease of TMR versus bias above 20 mV (Fig. 8) for the GaAs/AlAs/GaAs junction compared to the single AlAs barrier, which can be assigned to a gradual opening of a variety of chains including several localized states [from (iii)] adding itself to magnon excitations to destroy the spin memory during the tunnel processes.

V. CONCLUSION

In conclusion, Auger electron spectroscopy and transmission electron microscopy analyses allow us to determinate a Mn diffusion depth of 12 ± 3 Å at the $Ga_{1-x}Mn_xAs$/GaAs interface. Even if the insertion of a thin GaAs layer seems to prevent the Mn diffusion into the tunnel barrier and therefore enhance the TMR, the insertion of a GaAs thicker than the Mn diffusion depth induces the opening of a thermally activated non-spin-polarized channel and thus a fast decrease of the TMR with the temperature. Thus, GaAs spacer thickness appears to be a crucial component on the TMR temperature dependence of ferromagnetic semiconductor tunnel junctions.

ACKNOWLEDGMENTS

This research was supported by the French program Action concertée Nanosciences-Nanotechnologies and by the EU through the RTN "Computational Magnetoelectronics" (HPRN-CT-2000-00143).

*Electronic address: richard.mattana@thalesgroup.com
†Electronic address: jean-marie.george@thalesgroup.com

[1] *Semiconductor Spintronics and Quantum Computation*. edited by D. D. Awschalom, D. Loss and N. Samarth (Springer, Berlin, 2002).
[2] E. Y. Tsymbal, O. N. Mryasov, and P. R. LeClair, J. Phys.: Condens. Matter **15**, 109 (2003).
[3] T. Dietl, H. Ohno, F. Matsukura, J. Cibert, and D. Ferrand, Science **287**, 1019 (2000).
[4] T. Dietl, H. Ohno and F. Matsukura, Phys. Rev. B **63**, 195205 (2001).
[5] D. Chiba, N. Akiba, F. Matsukara, Y. Ohno, and H. Ohno, Appl. Phys. Lett. **77**, 1873 (2000).
[6] M. Tanaka, H. Shimizu, T. Hayashi, H. Shimada, and K. Ando, J. Vac. Sci. Technol. A **18**, 1247 (2000).
[7] F. Matsukura, H. Ohno, and T. Dietl, *Handbook of Magnetic Materials*, edited by K. H. J. Buschow (North-Holland, Amsterdam, 2002), Vol. 14, pp. 1–87.
[8] K. W. Edmonds, P. Bogusawski, K. Y. Wang, R. P. Campion, S. N. Novikov, N. R. S. Farley, B. L. Gallagher, C. T. Foxon, M. Sawicki, T. Dietl, M. Buongiorno Nardelli, and J. Bernholc, Phys. Rev. Lett. **92**, 037201 (2004).
[9] M. Tanaka and Y. Higo, Phys. Rev. Lett. **87**, 026602 (2001).
[10] R. Mattana, J.-M. George, H. Jaffrès, F. NGuyen Van Dau, A. Fert, B. Lépine, A. Guivarc'h, and G. Jézéquel, Phys. Rev. Lett. **90**, 166601 (2003).
[11] S. H. Chun, S. J. Potashnick, K. C. Ku, P. Schiffer, and N. Samarth, Phys. Rev. B **66**, 100408 (2002).
[12] A. Shen, F. Matsukura, S. P. Guo, Y. Sugawara, H. Ohno, M. Tani, H. Abe and H. C. Liu, J. Cryst. Growth **201-202**, 679 (1999).
[13] J. Sadowski, J. Z. Domagala, J. Bak-Misiuk, S. Kolesnik, K. Swiatek, J. Kanski, and L. Ilver, Thin Solid Films **367**, 165 (2000).
[14] The elastic moduli of GaAs are $C_{11}=118.9$ GPa and $C_{12}=53.8$ GPa, whereas the strain relation for a cubic unit cell is written $(a_\perp - a_0)/(a_\parallel - a_0) = -2C_{12}/C_{11} = -0.905$.
[15] G. M. Shott, W. Faschinger, and L. W. Molenkamp, Appl. Phys. Lett. **79**, 1807 (2001).
[16] J. Sadowski, R. Mathieu, P. Svedlindh, J. Z. Domagala, J. Bak-Misiuk, K. Swiatek, M. Karlsteen, J. Kanski, L. Ilver, H. Asklund, and U. Sodervall, Appl. Phys. Lett. **78**, 3271 (2001).
[17] H. Ohno, A. Shen, F. Matsukura, A. Oiwa, A. Endo, S. Katsumoto, and Y. Iye, Appl. Phys. Lett. **69**, 363 (1996).
[18] H. Ohno, J. Magn. Magn. Mater. **200**, 110 (1999).
[19] A. Kaminski, and S. Das Sarma, Phys. Rev. Lett. **88**, 247202 (2002).
[20] S. A. Schartz, C. R. Helms, W. E. Spicer, and N. J. Taylor, Report No. NBS.SP.400.67, National Bureau of Standards, Washington (1981).
[21] J. Olivier, F. Wyczisk, R. Bisaro, G. Padeletti, and J. Nagle, 5th Conf. on Appl. of Surf. and Interf. Analysis (ECASIA), Catania, Italy Oct. (1993).
[22] K. Kajiwara and R. Shimuzu, J. Vac. Sci. Technol. A **13**, 1316 (1995).
[23] C. Gould, C. Rüster, T. Jungwirth, E. Girgis, G. M. Schott, R. Giraud, K. Brunner, G. Schmidt, and L. W. Molenkamp, Phys. Rev. Lett. **93**, 117203 (2004).
[24] M. Jullière, Phys. Lett. **54A**, 225 (1975).
[25] Y. Ohno, I. Arata, F. Matsukura, and H. Ohno, Physica E (Amsterdam) **13**, 521 (2002).

[26] H. Åsklund, L. Ilver, J. Kanski, J. Sadowski, and R. Mathieu, Phys. Rev. B **66**, 115319 (2002).
[27] D. Chiba, F. Matsukura, and H. Ohno, Physica E (Amsterdam) **21**, 966 (2004).
[28] A. I. Larkin, and K. A. Matveev, Zh. Eksp. Teor. Fiz. **93**, 1030 (1987) [Sov. Phys. JETP **66**, 580 (1987)].
[29] L. I. Glazman, and R. I. Shekhter, Zh. Eksp. Teor. Fiz. **94**, 292 (1988) **67**, 163 (1988)].
[30] Y. Xu, D. Ephron, and M. R. Beasley, Phys. Rev. B **52**(4), 2843 (1995).
[31] R. M. Feenstra, J. M. Woodall and G. D. Pettit, Phys. Rev. Lett. **71** 1176 (1993).
[32] M. Stellmacher, R. Bisaro, P. Galtier, J. Nagle, and K. Khirouni, Semicond. Sci. Technol. **16** 440 (2001).
[33] S. Lodha, D. B. Janes, and N. P. Chen, J. Appl. Phys. **93**, 2772 (2003).
[34] Because of the Auger detection sensitivity limit, a Mn concentration in the barrier up to 10^{19} cm^{-3} is not excluded. However, the smooth decrease of TMR with temperature up to T_C ($\simeq$60 K) seems to indicate that the paramagnetic Mn impurities in the AlAs barrier do not play a crucial role for tunneling.
[35] J.-M. George, H. Jaffrès, R. Mattana, M. Elsen, F. NGuyen Van Dau, A. Fert, B. Lépine, A. Guivarc'h, and G. Jézéquel,, Mol. Phys. Rep. **40**, 23 (2004).
[36] In the limit where the characteristic time of spin flip by anisotropic exchange mechanism [K. V. Kavokin, Phys. Rev. B **64**, 075305 (2001)] is much larger than the dwell time of holes in the localized state.
[37] A. G. Petukhov, A. N. Chantis, and D. O. Demchenko, Phys. Rev. Lett. **89** 107205 (2002).
[38] E. Y. Tsymbal, A. Sokolov, I. F. Sabirianov, and B. Doudin, Phys. Rev. Lett. **90**, 186602 (2003).
[39] A. Fert and H. Jaffrès, Phys. Rev. B **64**(18), 184420 (2001).
[40] R. Mattana *et al.* (unpublished).